Journal of Materials Chemistry C

Accepted Manuscript

ROYAL SOCIETY OF CHEMISTRY

rsc.li/materials-c

DOI: 10.1039/C7TC00733G

Journal Name

ARTICLE

π-π stacking: a strategy to improve the electron mobilities of bipolar hosts for TADF and phosphorescent devices with low efficiency roll-off

Received 00th January 20xx,
Accepted 00th January 20xx

DOI: 10.1039/x0xx00000x

www.rsc.org/

Minghan Cai,[a] Xiaozeng Song,[a] Dongdong Zhang,[a] Juan Qiao[a] and Lian Duan*[a]

A series of D-π-A type bipolar hosts based on triphenylene/carbazole were designed and synthesized. π-π stacking of triphenylene units between two adjacent molecules renders these hosts high electron mobilities above 1×10^{-4} cm^2 V^{-1} s^{-1} and their electron and hole mobilities can be regulated through varying the connection position and π moieties. Due to more balanced charge mobilities, D1 based green thermally activated delayed fluorescence (TADF) device achieved the highest external quantum efficiency (EQE) of 16.3% and its EQE could still maintain 15.3% and 13.8% at high luminance of 5000 cd m^{-2} and 10000 cd m^{-2}, respectively. D1 based green phosphorescent devices also exhibited a highest EQE of 18.6% with reduced roll-off to 17.6% at 5000 cd m^{-2} and 16.2% at 10000 cd m^{-2}.

Introduction

Nowadays, organic light emitting diodes (OLEDs) have already become the most promising technology in display field due to their characteristics such as self-luminous, low power consumption, high resolution and high flexibility.[1] The utilization of excitons plays an important role in making OLED devices more efficient.[2] Compared with fluorescent materials which can merely use singlets to emit light, phosphorescent and TADF materials can utilize both singlets and triplets.[3-7] Recently developed phosphorescent and TADF materials can even achieve 100% internal quantum efficiencies (IQEs). However, the efficiency roll-off of most phosphorescent organic light emitting diodes (PHOLEDs) and TADF OLEDs is serious, especially in high luminance of 5000 cd m^{-2} and 10000 cd m^{-2}. Efficiency roll-off will not only increase power consumption but also shorten the lifetime of devices. Previous studies showed that efficiency roll-off could be ascribed to triplet-triplet annihilation (TTA) and triplet-polaron annihilation (TPA) caused by the long-lived triplets of emitters under high driving voltage and aggregation induced quenching (ACQ) phenomenon caused by high doping concentration of dopants.[8]

To suppress efficiency roll-off, phosphorescent and TADF materials are often dispersed in hosts to limit their intermolecular interaction. Our previous researches showed that hosts should possess sufficient high triplets, effective energy transfer to emitters, suitable highest occupied molecular orbital (HOMO) and lowest unoccupied molecular orbital (LUMO) energy levels.[9-14] Besides, balanced hole and electron mobilities of hosts are also crucial for high efficiency and long lifetime devices.[15-17] Bonding electron-donating and electron-accepting unit is a commonly used strategy for designing bipolar hosts with balanced electron and hole mobilities.[18-25] For example, Lee and his group synthesized bipolar host 3',5'-di(carbazol-9-yl)-[1,1'-biphenyl]-3,5-dicarbonitrile (DCzDCN) for both TADF and phosphorescent OLEDs. Efficiency roll-off of these devices had been significantly suppressed.[26]

Interestingly, bipolar hosts with equal electron and hole mobilities may not be the best choice. Adachi's group found that PHOLEDs using electron transporting layer materials as hosts exhibited higher efficiencies than reference device using bipolar host 4,4'-Bis-(9-carbazolyl)-biphenyl (CBP) as host.[27] Recently, they also confirmed that blue TADF OLEDs could be more stable if the emitters are doped into electron-transport materials instead of hole-transport materials as a result of reduced electrochemical oxidation process and a photo-oxidation process.[28] Besides, hole mobilities of most hole transporting materials (HTMs) are about two to three orders of magnitude higher than the electron mobilities of classical electron transporting materials (ETMs).[29] Bipolar hosts with relatively higher electron mobilities will be more compatible with adjacent charge transport layers. Thus, new strategies to further improve electron mobilities of bipolar hosts are highly desired.

Previous studies showed that interaction between adjacent molecules can significantly improve the electron mobilities.[30-32] π-π stacking is a kind of intermolecular interaction widely found in polycyclic aromatic derivatives. Besides, their HOMOs and LUMOs can be easily modulated by

*a.Key Lab of Organic Optoelectronics and Molecular Engineering of Ministry of Education, Department of Chemistry, Tsinghua University, Beijing 100084, China. *E-mail: duanl@mail.tsinghua.edu.cn; Fax: +86-10-62795137; Tel: +86-10-62782197.*

† Electronic Supplementary Information (ESI) available: See DOI: 10.1039/x0xx00000x

View Article Online
DOI: 10.1039/C7TC00733G

changing the fragments attaching to them. For example, triphenylene based materials usually tend to pile up by π-π stacking and show one-dimensional charge transporting properties. Conductivity along the columns is much higher than that in the perpendicular direction.[33-34] By attaching to pyridine, Adachi designed triphenylene-based ETM 2,7-Bis(2,2'-bipyridine-5-yl)triphenylene (Bpy-TP2). OLEDs containing Bpy-TP2 as ETM showed significantly lower driving voltages, lower power consumption and equal lifetime when compared with devices using conventional ETMs.[35] Besides, triphenylene derivatives can also be used as hosts.[36-38] By attaching to carbazole, Lee's group prepared triphenylene based host 4-(3-(triphenylen-2-yl)phenyl)dibenzo[b,d]thiophene (DBTTP1) for green TADF OLED and it achieved a high EQE above 20% with a long lifetime.[36] Lee and Jeon synthesised three triphenylene derivatives for the use as hosts for green PHOLEDs and achieved a high EQE up to 20.3%.[37] However, the relationship between intermolecular interaction, electron and hole mobilities and good device performance was still unclear in the above researches.

Here, we report six hosts D1-D6 for both TADF and phosphorescent OLEDs. Triphenylene was selected as n-type unit and carbazole was selected as p-type unit. Due to various connection position and π moieties, six hosts exhibit different hole and electron mobilities. We fabricated green TADF and phosphorescent devices using 1,2,3,5-tetrakis(carbazol-9-yl)-4,6-dicyanobenzene (4CzIPN) and tris[2-phenylpyridinato-C^2,N] iridium(III) [$Ir(ppy)_3$] as the dopants, respectively. Due to more balanced charge transport properties, D1 based TADF and phosphorescent devices exhibited the highest EQEs up to 16.3% and 18.6%, respectively. These values are higher than the EQEs of reference TADF device (11.5%) and phosphorescent device (15.8%) using CBP as the host. The efficiency roll-off of D1 based devices is also lower than that of CBP based device.

Experimental section

General information

The ^{1}H NMR spectra were measured by a JEOLAL-600 MHz spectrometer at ambient temperature with tetramethylsilane as the internal standard. The mass spectra were recorded on MALDI-TOF MS, Performance (Shimadzu, Japan). The thermogravimetric analysis (TGA) was performed on a STA 409PC thermogravimeter at a heating rate of 10 ^{o}C min^{-1} from ambient temperature to 600 ^{o}C under nitrogen atmosphere. The differential scanning calorimetry (DSC) measurements were performed on a DSC 2910 modulated calorimeter at a heating rate of 10 ^{o}C min^{-1} from ambient temperature to the temperature before decomposition under nitrogen atmosphere. The electrochemical measurements were performed with a Potentiostat/ Galvanostat Model 283 (Princeton Applied Research) electrochemical workstation by using Pt as working electrode, platinum wire as auxiliary electrode, and a Ag wire as reference electrode standardized against ferrocene/ ferrocenium. The oxidation potentials were measured in dichloromethane solution containing 0.1 M n-Bu_4NPF_6 as supporting electrolyte at a scan rate of 100 mV s^{-1}. The UV/Vis absorption spectra were recorded by an Agilent 8453 spectrophotometer. The quantum chemical calculations were performed by using the Gaussian 09 program package. The geometries of materials in the ground stat were optimized via density functional theory (DFT) calculations at the B3LYP/6-31G(d) level. Triplet states and singlet states of these materials were calculated by using time-dependent density functional theory (TD-DFT) calculations at B3LYP/6-31G(d) level. The HOMO and LUMO orbitals were visualized by using Gaussview. The surface morphologies of films were measured by SPA400 (Seiko instruments Inc.). Single crystals were grown from slow evaporation of dichloromethane/petroleum ether (1:4) solutions. The room temperature single-crystal X-ray experiments were performed on a RIGAKU SATURN 724+ CCD diffractometer equipped with a graphite monochromatized Mo Kα radiation. The structures were solved by direct methods and refined with a full-matrix least-squares technique based on F2 with the SHELXL-97 crystallographic software package. The corresponding CCDC reference numbers (CCDC: 1524760 and 1524763) and the data can be obtained free of charge from The Cambridge Crystallographic Data Centre.

Syntheses

Materials. 2-bromotriphenylene was purchased from the Shanghai Dibai Technology Co. Ltd. 2-(3-Bromophenyl)triphenylene was purchased from the Suzhou ge'ao New Material Co. Ltd. and all of the boronic acid ramifications were purchased from Beijing Pure Chem. Co. Ltd. All of these reagents were received and used without further purification.

General procedure for synthese of 9-(3-(triphenylen-11-yl)phenyl)-9H-carbazole and other products. 2-bromotriphenylene (2.15 g, 7.0 mmol), 3-(9H-Carbazol-9-yl)phenylboronic acid (2.00 g, 7.0 mmol), tetrakis(triphenylphosphine)palladium(0) (0.24 g, 0.21 mmol), 2M Na_2CO_3 (20 ml), ethanol (3 ml) and toluene (30 ml) were sequentially added to a 100 ml round-bottom flask. The mixture was heated to 80 ^{o}C and refluxed under nitrogen atmosphere for 48 hours. After the reaction completed, the mixture was extracted with 500 ml dichloromethane for two times. The organic layer was stored and evaporated under reduced pressure. Then, the crude product was isolated by silica gel column chromatography and further purified by vacuum sublimation to give pure product as white solid.

9-[3-(2-triphenylenyl)phenyl]-9H-Carbazole (D1). Yield: 76%. ^{1}H NMR (600 MHz, $CDCl_3$, TMS): δ= 8.89 (s, 1H), 8.71 (t, 2H), 8.66 (d, J=8Hz, 3H), 8.19 (d, J=8Hz, 2H), 8.02 (s, 1H), 7.92 (t, 2H), 7.76 (t, 1H), 7.70-7.65 (m, 3H), 7.63 (t, 2H), 7.54 (d, J=8Hz, 2H), 7.45 (t, 2H), 7.32 (t, 2H). ^{13}C NMR (150 MHz, $CDCl_3$): δ= 143.17, 141.05, 138.76, 138.52, 130.59, 130.31, 130.17, 130.01, 129.73, 129.56, 129.47, 127.62, 127.55, 127.48, 127.45, 126.52, 126.28, 126.23, 126.19, 126.06, 124.25,

View Article Online
DOI: 10.1039/C7TC00733G

123.57, 123.53, 123.49, 123.45, 121.95, 120.54, 120.17, 109.99. MS (MALDI-TOF): *m/z* 469.2710 $[M]^+$. Elemental analysis: calcd. for $C_{36}H_{23}N$: C, 92.08; H, 4.94; N, 2.98; found: C, 91.98; H, 4.90; N, 3.12.

9-[4-(2-triphenylenyl)phenyl]-9H-Carbazole (D2). Yield: 83%. ^{1}H NMR (600 MHz, $CDCl_3$, TMS): δ= 8.95 (s, 1H), 8.82-8.79 (m, 1H), 8.77(d, J=8Hz, 1H), 8.73-8.66 (m, 3H), 8.18 (d, J=8Hz, 2H), 8.03 (d, J=8Hz, 2H), 7.99 (d, J=8Hz, 1H), 7.73 (d, J=8Hz, 2H), 7.72-7.67 (m, 4H), 7.54 (d, J=8Hz, 2H), 7.46 (t, 2H), 7.32 (t, 2H). ^{13}C NMR (150 MHz, $CDCl_3$): δ= 141.00, 140.37, 139.04, 137.24, 130.35, 130.25, 130.02, 129.86, 129.67, 129.35, 128.94, 127.64, 127.54, 127.49, 126.37, 126.16, 124.27, 123.61, 123.55, 123.49, 121.99, 120.52, 120.18, 110.01. MS (MALDI-TOF): *m/z* 469.3142 $[M]^+$. Elemental analysis: calcd. for $C_{36}H_{23}N$: C, 92.08; H, 4.94; N, 2.98; found: C, 91.88; H, 5.01; N, 3.11.

9-phenyl-3-(2-triphenylenyl)-9H-Carbazole (D3). Yield: 80%. ^{1}H NMR (600 MHz, $CDCl_3$, TMS): δ= 8.96 (s, 1H), 8.82 (d, J=8Hz, 1H), 8.72 (d, J=8Hz, 1H), 8.69 (t, 3H), 8.55 (s, 1H), 8.28 (d, J=8Hz, 1H), 8.02 (d, J=8Hz, 1H), 7.86 (d, J=8Hz, 1H), 7.73-7.66 (m, 4H), 7.66-7.61 (m, 4H), 7.55 (d, J=8Hz, 1H), 7.53-7.48 (m, 1H), 7.46 (d, J=4Hz, 2H), 7.38-7.32 (m, 1H). ^{13}C NMR (150 MHz, $CDCl_3$): δ= 141.57, 140.88, 140.69, 137.78, 133.52, 130.32, 130.12, 128.51, 127.74, 127.45, 127.40, 127.26, 127.23, 126.89, 126.39, 125.87, 124.20, 124.03, 123.62, 123.57, 123.50, 123.46, 121.91, 120.65, 120.30, 119.26, 110.36, 110.14. MS (MALDI-TOF): *m/z* 469.3012 $[M]^+$. Elemental analysis: calcd. for $C_{36}H_{23}N$: C, 92.08; H, 4.94; N, 2.98; found: C, 92.02; H, 4.88; N, 3.10.

9-[3'-(2-triphenylenyl)[1,1'-biphenyl]-3-yl]-9H-Carbazole (D4). Yield: 68%. ^{1}H NMR (600 MHz, $CDCl_3$, TMS): δ= 8.94 (s, 1H), 8.91-8.77 (m, 1H), 8.76 (d, J=8Hz, 1H), 8.72-8.66 (m, 3H), 8.17 (d, J=8Hz, 2H), 8.11 (s, 1H), 7.99 (d, J=8Hz, 1H), 7.94 (d, J=8Hz, 2H), 7.85 (d, J=8Hz, 1H), 7.74 (d, J=8Hz, 1H), 7.72-7.65 (m, 7H), 7.52 (d, J=8Hz, 2H), 7.44 (t, 2H), 7.31 (t, 2H). ^{13}C NMR (150 MHz, $CDCl_3$): δ= 142.12, 141.22, 140.98, 140.37, 139.83, 137.24, 130.30, 130.22, 129.99, 129.90, 129.73, 129.27, 128.87, 127.59, 127.56, 127.50, 127.45, 126.92, 126.58, 126.50, 126.14, 124.16, 123.59, 123.58, 123.54, 123.52, 122.07, 120.50, 120.16, 109.99. MS (MALDI-TOF): *m/z* 545.3247 $[M]^+$. Elemental analysis: calcd. for $C_{42}H_{27}N$: C, 92.45; H, 4.99; N, 2.57; found: C, 92.20; H, 4.91; N, 2.89.

9-[3'-(2-triphenylenyl)[1,1'-biphenyl]-4-yl]-9H-Carbazole (D5). Yield: 73%. ^{1}H NMR (600 MHz, $CDCl_3$, TMS): δ= 8.89 (s, 1H), 8.76-8.73 (m, 1H), 8.71 (d, J=8Hz, 1H), 8.69-8.64 (m, 3H), 8.18 (d, J=8Hz, 2H), 8.05 (s, 1H), 7.93 (d, J=7Hz, 2H), 7.82 (d, J=8Hz, 2H), 7.73 (t, 1H), 7.71-7.59 (m, 7H), 7.53 (d, J=8Hz, 2H), 7.45 (t, J=2Hz, 2H), 7.32 (t, J=2Hz, 2H). ^{13}C NMR (150 MHz, $CDCl_3$): δ= 143.25, 142.11, 141.08, 140.99, 139.68, 138.44, 130.53, 130.27, 130.17, 129.96, 129.86, 129.73, 129.67, 129.24, 127.56, 127.47, 127.11, 126.54, 126.48, 126.17, 126.02, 124.14, 123.56, 123.52, 122.00, 120.52, 120.16, 109.97. MS (MALDI-TOF): *m/z* 545.2889 $[M]^+$. Elemental analysis: calcd. for $C_{42}H_{27}N$: C, 92.45; H, 4.99; N, 2.57; found: C, 92.33; H, 5.01; N, 2.66.

9-phenyl-3-[3-(2-triphenylenyl)phenyl]-9H-Carbazole (D6). Yield: 80%. ^{1}H NMR (600 MHz, $CDCl_3$, TMS): δ= 8.96 (s, 1H), 8.81-8.75 (m, 2H), 8.73-8.66 (m, 3H), 8.49-8.47 (s, 1H), 8.26-8.22 (d, J=8Hz, 1H), 8.16-8.13 (s, 1H),8.03-7.99 (d, J=9Hz, 1H), 7.82-7.76 (m, 3H), 7.72-7.60 (m, 9H), 7.55-7.48 (m, 2H), 7.47-7.42 (m, 2H), 7.36-7.31 (m, 1H). ^{13}C NMR (150 MHz, $CDCl_3$): δ= 142.90, 141.90, 141.50, 140.62, 140.16, 137.74, 133.49, 130.24, 130.16, 130.08, 129.93, 129.74, 129.53, 129.11, 127.69, 127.50, 127.44, 127.41, 127.39, 127.21, 126.74, 126.71, 126.65, 126.34, 125.87, 125.75, 124.07, 123.57, 123.51, 123.49, 122.06, 120.59, 120.26, 119.14, 110.26, 110.09. MS (MALDI-TOF): *m/z* 545.3032 $[M]^+$. Elemental analysis: calcd. for $C_{42}H_{27}N$: C, 92.45; H, 4.99; N, 2.57; found: C, 92.40; H, 4.98; N, 2.62.

Device fabrication and measurements

Besides the synthesized materials, all other reagents used in fabricating devices were purchased from Jilin Optical and Electronic Materials Co. Ltd. and Xi'an Polymer Light Technology Co. Ltd. The organic layers were deposited consecutively on the precleaned ITO-coated glass substrates in a vacuum chamber with a pressure of 2×10^{-4} Torr. Next, the cathode was fabricated with thermal evaporation of a 0.5 nm LiF layer followed by a 150 nm aluminum layer. The deposition rates of all organic materials and aluminum were 1-2 Å s^{-1}, while that of the LiF layer was 0.1 Å s^{-1}. The electrical characteristics of the devices were measured with Keithley 2400 source meter. The electroluminescence spectra and luminance of the devices were obtained on a PR650 spectrometer. Characteristics of all the OLED devices were carried out in ambient laboratory conditions at room temperature.

Results and discussion

Synthesis and characterization

Bipolar hosts D1-D6 were synthesized by Suzuki coupling reaction. The synthetic routes and chemical structures of all hosts are shown in Scheme 1. All reagents were commercially available and used as obtained. ^{1}H nuclear magnetic resonance (^{1}H NMR) spectrometer and mass spectrometry were used to characterize the molecular structures.

Thermal and morphology properties

We employed TGA and DSC tests to investigate the thermal properties of D1-D6. The results are shown in Fig. 1 and Fig. S1 (ESI†). Compared with traditional host CBP, D1-D3 show higher glass-transition temperatures (Tg) of 102, 111 and 107 °C, respectively. Among D1-D3, the liner shape D2 demonstrates the highest Tg. By introducing an extra phenyl group, the glass-transition temperatures of D1-D3 are further improved to 124, 114 and 120 °C for D4-D6, respectively. The thermal-decomposition temperatures (Td, corresponding to 5% weight

View Article Online
DOI: 10.1039/C7TC00733G

loss) of D1-D3 are 399, 374 and 369 °C, respectively. Similar to Tg, Td of D4-D6 increase to 409, 425 and 421 °C, respectively. Surface morphology of vacuum-deposited D1-D6 films were also measured by atomic force microscopy (AFM) (Fig. S2, ESI†). We observed no aggregation and crystallization for all of six hosts and the root-mean-square (RMS) roughness values of D1-D6 are 0.94, 1.05, 0.94, 1.01, 0.93 and 1.18 nm, respectively. Good thermostabilities and film-forming properties of D1-D6 can improve the stability and performances of devices.

DFT simulation

The HOMOs and the LUMOs of D1-D6 are simulated at B3LYP/6-31G(d) level by Gaussian 09 and presented in Fig. 2. DFT calculations confirm that the LUMOs of six hosts mainly localize on their triphenylene groups while the HOMOs of D1, D4, D5 and D6 mainly localize on their carbazole groups. Whereas, for D2, compared with D1, attaching the carbazole at para-position extends the location of HOMO from carbazole to triphenylene through the central phenyl. This phenomena is further strengthened by directly attaching carbazole at 3-position to triphenylene in D3, whose HOMO disperses to the whole molecular. Separately location of LUMOs and HOMOs usually induce intramolecular charge transfer (ICT). Thus, Compared with D2 and D3, D1, D4, D5 and D6 possess special absorption and fluorescence characters. This will be discussed in the following part.

Photophysical properties

UV/Vis absorption, photoluminescence (PL) and phosphorescence spectra of D1-D6 in toluene (1×10^{-5} mol L^{-1}) are shown in Fig. 3 and summarized in Table 1. We first consider the absorption spectra of these compounds. All six materials peak at about 290 nm. This is in accordance with many previous reported carbazole based compounds and can be assigned to the carbazole centered π-π* transitions.[39-41] The wide featureless emission at 300-320 nm of D1-D6 can be ascribed to the π-π* transitions between the carbazole units and the phenyl units connecting to them. Interestingly, weak absorption peaks can also be observed at 341, 345, 345 and 349 nm for D1, D4, D5 and D6, respectivly. This confirms the existence of charge transfer (CT) states which are usually found in D-A type molecules, like TADF materials whose HOMOs mainly localize on donor groups and LUMOs mainly localize on acceptor groups. DFT calculation results in Fig. 2 can support this idea. LUMOs of six hosts localize mainly on triphenylene but the location of their HOMOs expand from carbazole to triphenylene in the order of D1, D4, D5, D6 to D2 to D3. Thus, only D1, D4, D5 and D6 with significant HOMO and LUMO separation show this peaks. Upon photoexcitation at 300 nm, we recorded PL spectra of D1-D6 in toluene. The emission of D1, D4, D5 and D6 in toluene is almost the same and two peak at about 367 and 378 nm can be recognized. D2 and D3 peak at 371/386 nm and 376/394 nm. We also recorded spectra of D1-D6 in tetrahydrofuran and dichloromethane for comparison (Fig. S3, ESI†). Replacement of toluene by more polar solvents cannot influence the location but merely change the relative strength of two peaks for all compounds except for D2. This result suggests that, although there exist CT states in D1, D4, D5 and D6. Locally excited (LE) states still dominate. In film, D1, D2 and D3 all peak at 401 nm (Fig. S4, ESI†). For D4, D5 and D6 the including of another phenyl introduces large steric hindrance and increases the distance between two adjacent molecules. This results in the blue shift of PL emission peaks from 401 nm of D1, D2 and D3 to 388, 378 and 390 nm of D4, D5 and D6, respectively. The triplet energies of D1-D6 were determined by their first phosphorescence peaks recorded in toluene solution at 77 K. Similar to their fluorescence spectra in toluene, D1, D4, D5 and D6 show a much higher triplet energies of 2.66, 2.67, 2.66 and 2.65 eV, respectively. And the triplet energies of D2 and D3 are 2.60 and 2.61 eV. High triplet energies make D1-D6 suitable hosts for green dopants.

Electrochemical properties

The electrochemical properties of D1-D6 were investigated by cyclic voltammetry (CV). As shown in Fig. 4, all of these compounds show excellent oxidation behaviors. This is due to the introduction of carbazole group. The HOMO levels of D1-D6 are determined from the onset of the 1st oxidation potentials with regard to the energy level of ferrocene and the LUMO levels are calculated by adding the optical band gap to the HOMO levels. The estimated HOMO levels of D1, D2 and D3 are 5.67, 5.63 and 5.54 eV, respectively. Compare with D1, the enlarged distribution of HOMO shifts the HOMO levels of D2 and D3 to shallower levels. These values are similar to previously reported triphenylene and carbazole based host materials.[36, 37] As for D4, D5 and D6, their HOMO distribution is similar to D1. The introducing of extra phenyl causes slight increase of HOMO levels (5.65 eV for D4 and D5, 5.63 eV for D6). Optical band gaps of D1-D6 are estimated by the onset of their absorption spectra in Fig. 4. They are 3.57, 3.50, 3.44, 3.55, 3.75 and 3.45 eV for D1-D6, respectively. LUMO levels are calculated by HOMO levels and optical band gaps. The LUMO levels of D1-D6 are 2.10, 2.13, 2.10, 2.10, 2.08 and 2.18 eV, respectively. Except for D6, all hosts show almost identical LUMO levels. This is because the LUMOs of six hosts mainly localize on their triphenylene groups and are less more likely to be affected by the groups attaching to them. The variation trend of HOMOs and LUMOs of D1-D6 is accord with that of the calculated values (Fig. S5, ESI†). This result also validates the accuracy of our theoretical calculations.

Charge-transporting properties

We used time of flight (TOF) transient photocurrent measurements to investigate the charge-transporting properties of D1-D6. And the results are presented in Fig. 5. All of the mobility data could be well fitted with the Poole-Frenkel function of $\mu = \mu_0 \exp(E^{1/2}/\sigma)$. By adopting these equations, we acquired the hole and electron mobilities of D1-D6 at the electric field of 6×10^7 V m^{-1} for comparison (Fig. S6, ESI†). As we anticipated, electron mobilities of all hosts are high and

View Article Online
DOI: 10.1039/C7TC00733G

range from 1.02×10^{-4} to 9.66×10^{-4} cm^2 V^{-1} s^{-1}. Among these hosts, D2 shows the highest electron mobility of 9.66×10^{-4} cm^2 V^{-1} s^{-1}. Usually, para-isomer will show enhanced mobility over the meta-isomer. This can also be concluded from the single crystal structures and molecular packing data of D1 and D2 (Fig. 6). The triphenylene groups and carbazole groups of D1 and D2 have a dominating influence on the overall molecule stacking and this eventually affect their hole and electron mobilities. For both of them, their triphenylene groups tend to pile up along a specific direction. On the one hand, the carbazole groups of two adjacent D1 moleculars are not in the same side and they will rotate to locate on two sides and result in a "stair" like configuration. On the other hand, the carbazole groups of D2 will align along the direction that triphenylene groups pile up. Given that carbazole groups can transport holes efficiently, triphenylene can transport electrons efficiently and the distance between two adjacent D2 molecules is merely 3.3 Å. HOMO and LUMO orbitals of nearby D2 molecules will separately overlap to form two channels to delivery holes and electrons and lead to the high hole and electron mobilities of 2.87×10^{-4} and 9.66×10^{-4} cm^2 V^{-1} s^{-1}. Whereas for D1, the distance between two adjacent triphenylene groups are 3.4/2.8 Å and the distance between two adjacent carbazole groups is 4.7 Å. The relatively larger distance decrease the change for charges to hope and cause a lower mobilities of 5.53×10^{-5} cm^2 V^{-1} s^{-1} for hole and 2.17×10^{-4} cm^2 V^{-1} s^{-1} for electron. For D3, its hole mobility is 4.82×10^{-6} cm^2 V^{-1} s^{-1}, which is much lower than that of D1 and D2. This is because that the dispersion of HOMO and overlapping with LUMO usually lead to a decrease in hole mobility. The electron mobility of D3 is 3.45×10^{-4} cm^2 V^{-1} s^{-1} and is between the values of D1 and D2. As for D4, D5 and D6, the inducing of phenyl significantly influence their charge transport properties. Electron mobilities of D4, D5 and D6 are 2.52×10^{-4}, 1.74×10^{-4} and 1.02×10^{-4} cm^2 V^{-1} s^{-1}, which are much lower than those of D1, D2 and D3 respectively. This can be ascribe to the inclusion of extra phenyl will increase the steric hindrance and thus increase the distance of two nearby molecules which can suppress electrons to hop.

Devices

To verify the performance of six materials, we fabricated green TADF OLEDs (A1-A6) and PHOLEDs (B1-B6) containing D1-D6 as hosts, respectively. Two reference devices using CBP as host were also fabricated (R1 for TADF device and R2 for PHOLED). Devices structures are presented in Fig. 7. We used indium tin oxide (ITO) as an anode, hexaazatriphenylene hexacarbonitrile (HAT-CN) as a hole-injection layer, N,N'-bis(1-naphthyl)N,N'-diphenyl-1,1'-biphenyl-4,4'-diamine (NPB) as a hole-transport layer, TCTA as exciton/electron blocking layers, new synthesized six materials as host materials for emitting layers and $Ir(ppy)_3$ and 4CzIPN as dopant materials for emitting layers. 4,7-diphenyl-1,10-phenanthroline (Bphen) as electron transport layer and hole bloking layer, lithium fluoride (LiF) as an electron injection layer, Al as a cathode.

We optimized the dopant concentrations and the thickness of different layers. Structure of ITO/HAT-CN (20nm)/NPB (40nm)/TCTA (10nm)/HOST: 4CzIPN (10 wt%, 25nm)/Bphen (35nm)/LiF (1 nm)/Al (150nm) was adopted for green TADF OLEDs and structure of ITO/HAT-CN (20nm)/NPB (40nm)/TCTA (10nm)/HOST: $Ir(ppy)_3$ (5 wt%, 25nm)/Bphen (35nm)/LiF (1 nm)/Al (150nm) was adopted for green phosphorescent devices.

The electroluminance (EL) spectra, power efficiencies (PEs), current efficiencies (PEs), EQEs and current density–voltage–luminance (J-V-L) characteristics of TADF OLEDs based on six hosts are shown in Fig. 8 and summarized in Table 2. Due to the complete energy transfer, we observed no emission of hosts for all devices. The EL spectra of device A1, A2, A4 and A5 peak at around 533 nm. For device A3 and A6, they are 547 nm and 550 nm. The red shift spectra of device A3 and A6 are ascribe to the formation of exciplexes of D3 and D6 with 4CzIPN. To confirm this, we measured the PL spectra of 10 wt% 4CzIPN doped D1-D6 films (Fig. S7, ESI†). 4CzIPN doped D1, D2, D4 and D5 films all peak at 522 nm. Whereas, the peaks of 4CzIPN doped D3 and D6 films exhibit redshift to 530 nm and 527 nm, respectively. In addition to that, the spectra of 4CzIPN doped D3 and D6 films are broader than those of 4CzIPN doped D1, D2, D4 and D5 films. This further validates the formation of exciplexes between them. The turn on voltages (V_{on}) of device A1, A2, A4 and A5 are in the range of 3.1-3.6 V and the turn on voltages of A3 and A6 are 2.9 V and 2.7 V. The lower turn on voltages of A3 and A6 are attributed to the relatively shallower HOMOs of D3 and D6 and the formation of exciplexes (Fig. S8, ESI†). The maximum EQEs of device A1, A2, A4 and A5 are 16.3, 15.9, 15.4 and 15.5% and their maximum power efficiencies are 36.4, 41.4, 37.5 and 35.4 lm/W, respectively. These devices also show small efficiency roll-off to 15.3, 14.2, 14.3, 14.0% and 13.8, 12.4, 12.9, 12.4% at high luminance of 5000 cd m^{-2} and 10000 cd m^{-2}. Whereas, due to the formation of exciplexes, device A3 and A6 show much lower maximum EQEs of 5.5% and 12.3% and their EQEs significant decrease to 3.6%, 11.1% and 2.7%, 9.9% at 5000 cd m^{-2} and 10000 cd m^{-2}, respectively. Compared with device A1, A2, A4 and A5, reference device R1 using CBP as the host for 4CzIPN exhibited lower EQE and suffered from more serious efficiency roll-off.

When considering the efficiencies of A1 and A2 with A4 and A5, A1 and A2 using D1 and D2 as hosts showed best performances. This is due to more balanced electron and hole mobilities of D1 and D2 when compared with other hosts and their electron mobilities are slightly higher than their hole mobilities. Given that the hole mobility of TCTA is 3.0×10^{-3} cm^2 V^{-1} s^{-1} and electron mobility of Bphen is 5.2×10^{-4} cm^2 V^{-1} s^{-1}, D1 and D2 with slightly higher electron mobilities will be more compatible with adjacent layers and enhance the performances of devices.

We also fabricated PHOLEDs B1-B6 using D1-D6 as hosts for green phosphorescent dopant $Ir(ppy)_3$. All properties are shown in Fig. 9 and summarized in Table 2. Energy diagram of green PHOLEDs can be found in Fig. S9 (ESI†). They all show identical EL spectra with λmax = 517nm. The maximum EQEs of

View Article Online
DOI: 10.1039/C7TC00733G

devices B1-B6 are 18.6%, 17.3%, 16.2%, 16.8%, 15.7% and 16.4%, respectively. Unlike TADF OLEDs, all PHOLEDs show similar roll-off. Their EQEs can still remain 17.6%, 16.5%, 15.3%, 15.5%, 14.0%, 16.0% and 16.2%, 15.3%, 14.2%, 14.1%, 12.8%, 15.1% at high luminance of 5000 cd m^{-2} and 10000 cd m^{-2}, respectively. Similar to TADF OLEDs, performances of B1 and B2 using D1 and D2 as hosts achieved higher efficiencies than that of CBP based PHOLED device R2. The turn on voltages of six devices range from 3.7-4.4 V.

Conlusion

In summary, we designed and synthesized six carbazole/triphenylene based hosts. They all show good thermostability and film-forming property. π-π stacking of triphenylene units renders these bipolar hosts with high electron mobilities in the range of 1.02×10^{-4} to 9.66×10^{-4} cm^2 V^{-1} s^{-1} at 6×10^7 V m^{-1}. Among the six hosts, D1 and D2 show slightly higher electron mobilities than their corresponding hole mobilities and this make them promising host candidates. Compare with CBP and other hosts, TADF and phosphorescent OLEDs using D1 as the hosts achieved higher maximum EQEs of 16.3% and 18.6%. Even at very high luminance of 10000 cd m^{-2}, the efficiencies could still maintain 13.8% and 16.2%. The result show the great potential that π-π stacking can be used to improve electron mobilities of bipolar hosts for TADF and phosphorescent devices with low efficiency roll-off. More efficient TADF and phosphorescent hosts can be readily designed by using this stratagem.

Acknowledgements

We would like to thank the National Key R&D Program of China (Grant Nos. 2016YFB0400702 and 2016YFB0401003), the National Key R&D Program of China (Grant No. 2015CB655002) and the CAS "Interdisciplinary Innovation Team" for financial support.

Notes and references

1 C. W. Tang and S. A. VanSlyke, *Appl Phys Lett*, 1987, **51**, 913-915.
2 A. Chihaya, *Jpn J Appl Phys*, 2014, **53**, 060101.
3 Y. Ma, H. Zhang, J. Shen and C. Che, *Synthetic Met*, 1998, **94**, 245-248.
4 M. A. Baldo, D. F. O'Brien, Y. You, A. Shoustikov, S. Sibley, M. E. Thompson and S. R. Forrest, *Nature*, 1998, **395**, 151-154.
5 H. Uoyama, K. Goushi, K. Shizu, H. Nomura and C. Adachi, *Nature*, 2012, **492**, 234-238.
6 Y. Tao, K. Yuan, T. Chen, P. Xu, H. Li, R. Chen, C. Zheng, L. Zhang and W. Huang, *Advanced Materials*, 2014, **26**, 7931-7958.
7 D. Zhang, M. Cai, Y. Zhang, D. Zhang and L. Duan, *Materials Horizons*, 2016, **3**, 145-151.
8 C. Xiang, X. Fu, W. Wei, R. Liu, Y. Zhang, V. Balema, B. Nelson and F. So, *Adv Funct Mater*, 2016, **26**, 1463-1469.
9 D. Zhang, L. Duan, C. Li, Y. Li, H. Li, D. Zhang and Y. Qiu, *Advanced Materials*, 2014, **26**, 5050-5055.
10 D. Zhang, L. Duan, Y. Li, H. Li, Z. Bin, D. Zhang, J. Qiao, G. Dong, L. Wang and Y. Qiu, *Adv Funct Mater*, 2014, **24**, 3551-3561.
11 D. Zhang, L. Duan, Y. Zhang, M. Cai, D. Zhang and Y. Qiu, *Light Sci Appl*, 2015, **4**, e232.
12 D. Zhang, L. Duan, D. Zhang and Y. Qiu, *Journal of Materials Chemistry C*, 2014, **2**, 8983-8989.
13 D. Zhang, L. Duan, D. Zhang, J. Qiao, G. Dong, L. Wang and Y. Qiu, *Organic Electronics*, 2013, **14**, 260-266.
14 D. Zhang, M. Cai, Z. Bin, Y. Zhang, D. Zhang and L. Duan, *Chemical Science*, 2016, **7**, 3355-3363.
15 Y. Sun, L. Duan, D. Zhang, J. Qiao, G. Dong, L. Wang and Y. Qiu, *Adv Funct Mater*, 2011, **21**, 1881-1886.
16 L. Duan, J. Qiao, Y. Sun and Y. Qiu, *Advanced Materials*, 2011, **23**, 1137-1144.
17 D. Zhang, M. Cai, Y. Zhang, D. Zhang and L. Duan, *Acs Appl Mater Interfaces*, 2015, **7**, 28693-28700.
18 X. Ban, W. Jiang, K. Sun, X. Xie, L. Peng, H. Dong, Y. Sun, B. Huang, L. Duan and Y. Qiu, *Acs Appl Mater Interfaces*, 2015, **7**, 7303-7314.
19 C.-C. Lai, M.-J. Huang, H.-H. Chou, C.-Y. Liao, P. Rajamalli and C.-H. Cheng, *Adv Funct Mater*, 2015, **25**, 5548-5556.
20 J. Zhao, G.-H. Xie, C.-R. Yin, L.-H. Xie, C.-M. Han, R.-F. Chen, H. Xu, M.-D. Yi, Z.-P. Deng, S.-F. Chen, Y. Zhao, S.-Y. Liu and W. Huang, *Chem Mater*, 2011, **23**, 5331-5339.
21 M.-S. Lin, S.-J. Yang, H.-W. Chang, Y.-H. Huang, Y.-T. Tsai, C.-C. Wu, S.-H. Chou, E. Mondal and K.-T. Wong, *J Mater Chem*, 2012, **22**, 16114-16120.
22 W. Li, J. Li, D. Liu, F. Wang and S. Zhang, *Journal of Materials Chemistry C*, 2015, **3**, 12529-12538.
23 F.-P. Wu, Y.-M. Xie, L.-S. Cui, X.-Y. Liu, Q. Li, Z.-Q. Jiang and L.-S. Liao, *Synthetic Met*, 2015, **205**, 11-17.
24 J. Xiao, X.-K. Liu, X.-X. Wang, C.-J. Zheng and F. Li, *Organic Electronics*, 2014, **15**, 2763-2768.
25 X. Yin, T. Zhang, Q. Peng, T. Zhou, W. Zeng, Z. Zhu, G. Xie, F. Li, D. Ma and C. Yang, *Journal of Materials Chemistry C*, 2015, **3**, 7589-7596.
26 Y. J. Cho, K. S. Yook and J. Y. Lee, *Advanced Materials*, 2014, **26**, 4050-4055.
27 C. Adachi, M. A. Baldo, S. R. Forrest and M. E. Thompson, *Appl Phys Lett*, 2000, **77**, 904-906.
28 L.-S. Cui, Y.-L. Deng, D. P.-K. Tsang, Z.-Q. Jiang, Q. Zhang, L.-S. Liao and C. Adachi, *Advanced Materials*, 2016, **28**, 7620-7625.
29 J.-H. Jou, S. Kumar, A. Agrawal, T.-H. Li and S. Sahoo, *Journal of Materials Chemistry C*, 2015, **3**, 2974-3002.
30 T. Kamata, H. Sasabe, Y. Watanabe, D. Yokoyama, H. Katagiri and J. Kido, *Journal of Materials Chemistry C*, 2016, **4**, 1104-1110.
31 Y. Watanabe, H. Sasabe, D. Yokoyama, T. Beppu, H. Katagiri, Y.-J. Pu and J. Kido, *Advanced Optical Materials*, 2015, **3**, 769-773.
32 Y. Watanabe, H. Sasabe, D. Yokoyama, T. Beppu, H. Katagiri and J. Kido, *Journal of Materials Chemistry C*, 2016, **4**, 3699-3704.

View Article Online
DOI: 10.1039/C7TC00733G

33 E. Tritto, R. Chico, G. Sanz-Enguita, C. L. Folcia, J. Ortega, S. Coco and P. Espinet, *Inorg Chem*, 2014, **53**, 3449-3455.
34 J. Shi, Y. Wang, M. Xiao, P. Zhong, Y. Liu, H. Tan, M. Zhu and W. Zhu, *Tetrahedron*, 2015, **71**, 463-469.
35 K. Togashi, S. Nomura, N. Yokoyama, T. Yasuda and C. Adachi, *J Mater Chem*, 2012, **22**, 20689-20695.
36 Y. Im, W. Song and J. Y. Lee, *Journal of Materials Chemistry C*, 2015, **3**, 8061-8065.
37 N.-J. Lee, J. H. Jeon, I. In, J.-H. Lee and M. C. Suh, *Dyes Pigments*, 2014, **101**, 221-228.
38 1. S. N. Park, H. W. Lee, Y. S. Kim, J. Kim, S. E. Lee, H. W. Lee, Y. K. Kim and S. S. Yoon, *Synthetic Met*, 2015, **206**, 124-130.
39 S. A. Bagnich, A. Rudnick, P. Schroegel, P. Strohriegl and A. Köhler, Philosophical Transactions of the Royal Society A: Mathematical, Physical and Engineering Sciences, 2015, **373**.
40 S. A. Bagnich, S. Athanasopoulos, A. Rudnick, P. Schroegel, I. Bauer, N. C. Greenham, P. Strohriegl and A. Köhler, *The Journal of Physical Chemistry C*, 2015, **119**, 2380-2387.
41 K.-R. Wee, Y.-J. Cho, S. Jeong, S. Kwon, J.-D. Lee, I.-H. Suh and S. O. Kang, *J Am Chem Soc*, 2012, **134**, 17982-17990.

View Article Online
DOI: 10.1039/C7TC00733G

Scheme 1 Synthesis routes and chemical structures of D1-D6.

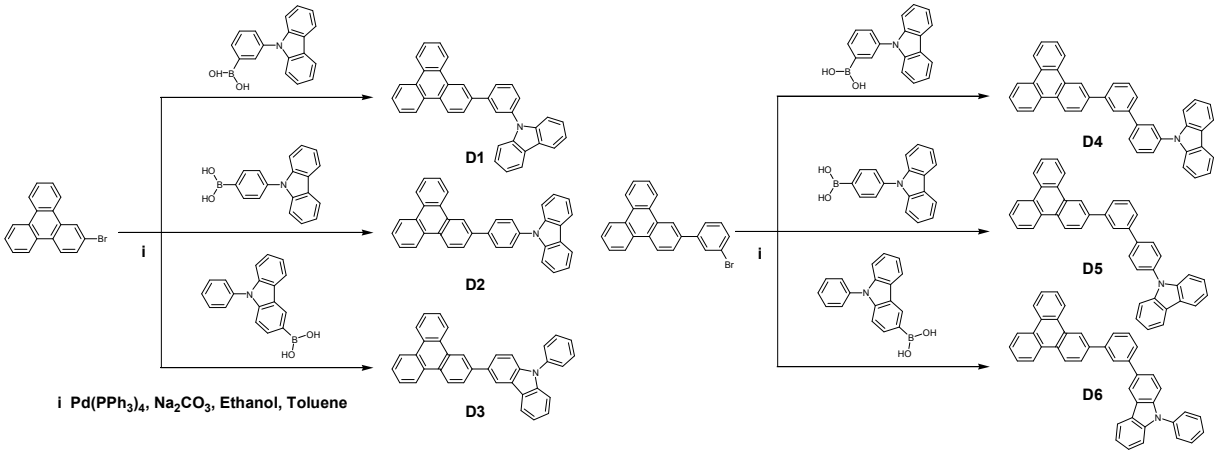

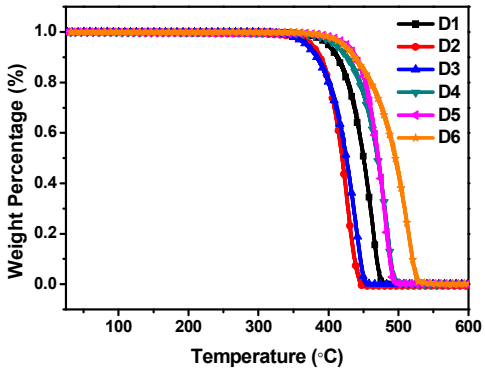

Fig. 1 TGA spectra of D1-D6.

View Article Online
DOI: 10.1039/C7TC00733G

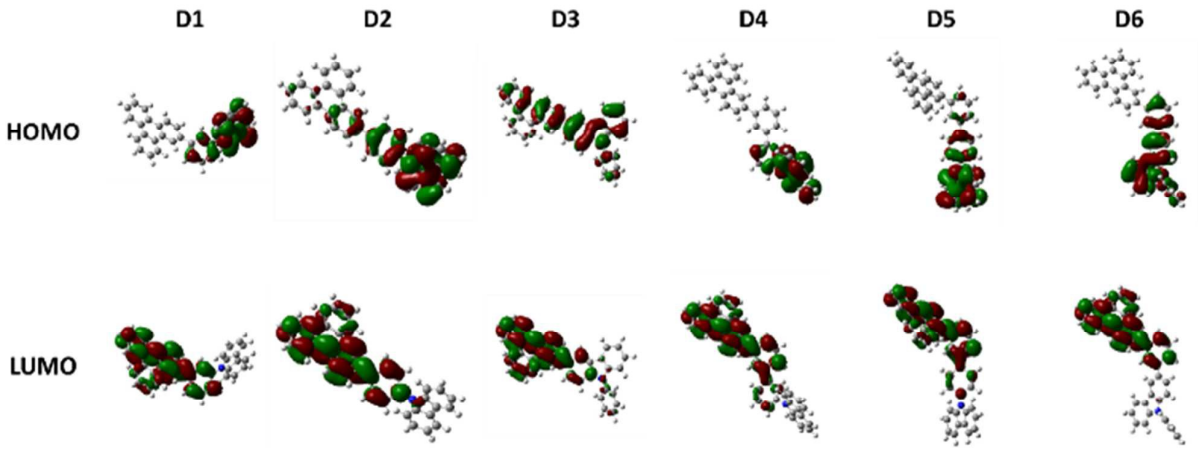

Fig. 2 HOMOs and LUMOs of D1-D6.

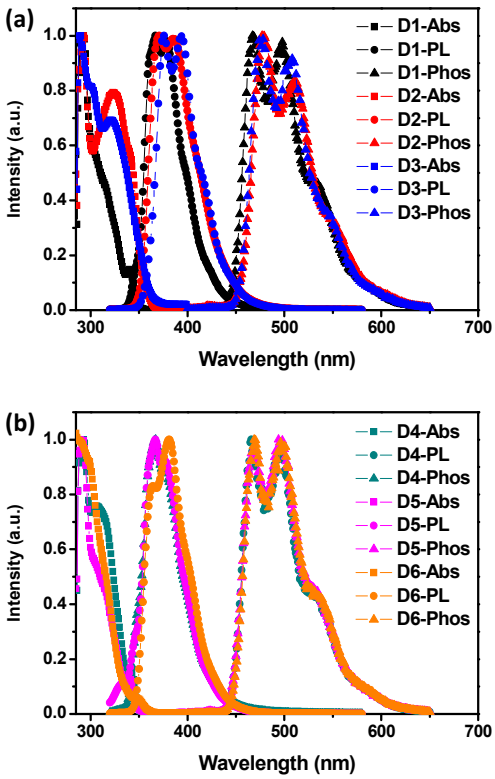

Fig. 3 UV/Vis absorption, PL and phosphorescence spectra of (a) D1-D3 and (b) D4-D6 in toluene.

View Article Online
DOI: 10.1039/C7TC00733G

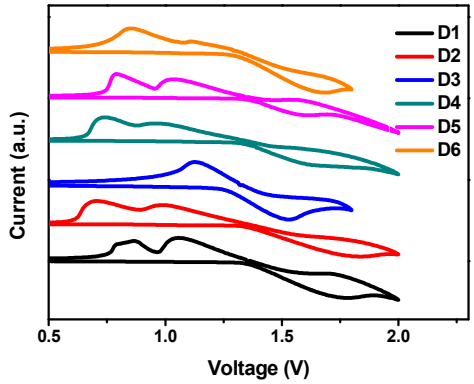

Fig. 4 Cyclic voltammograms of D1-D6 in ultra-dry dichloromethane.

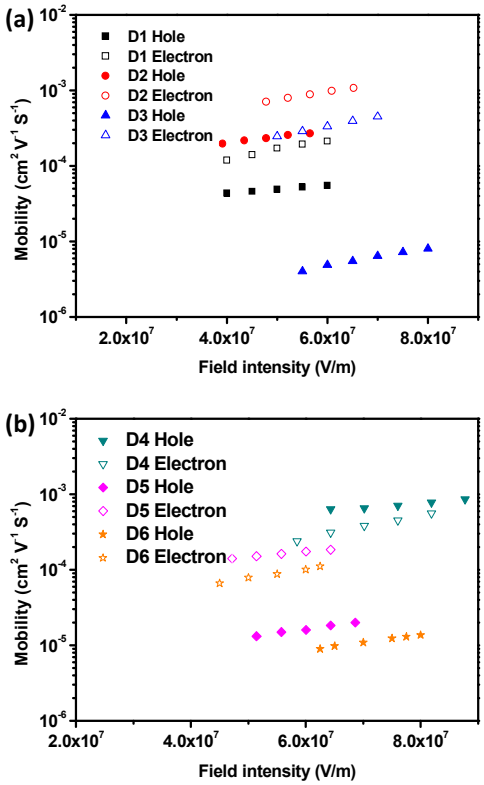

Fig. 5 Charge mobilities of (a) D1-D3 and (b) D4-D6 under different electric fields.

View Article Online
DOI: 10.1039/C7TC00733G

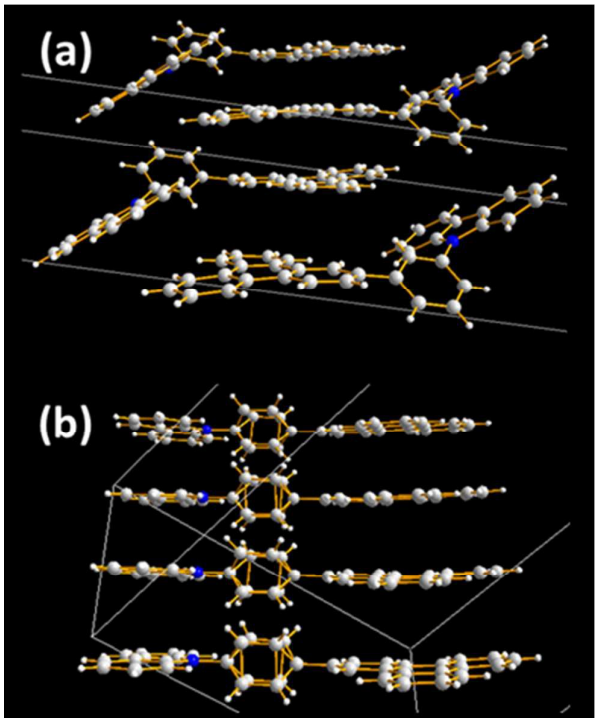

Fig. 6 Single crystal structures and molecular packing data of (a) D1 and (b) D2.

View Article Online
DOI: 10.1039/C7TC00733G

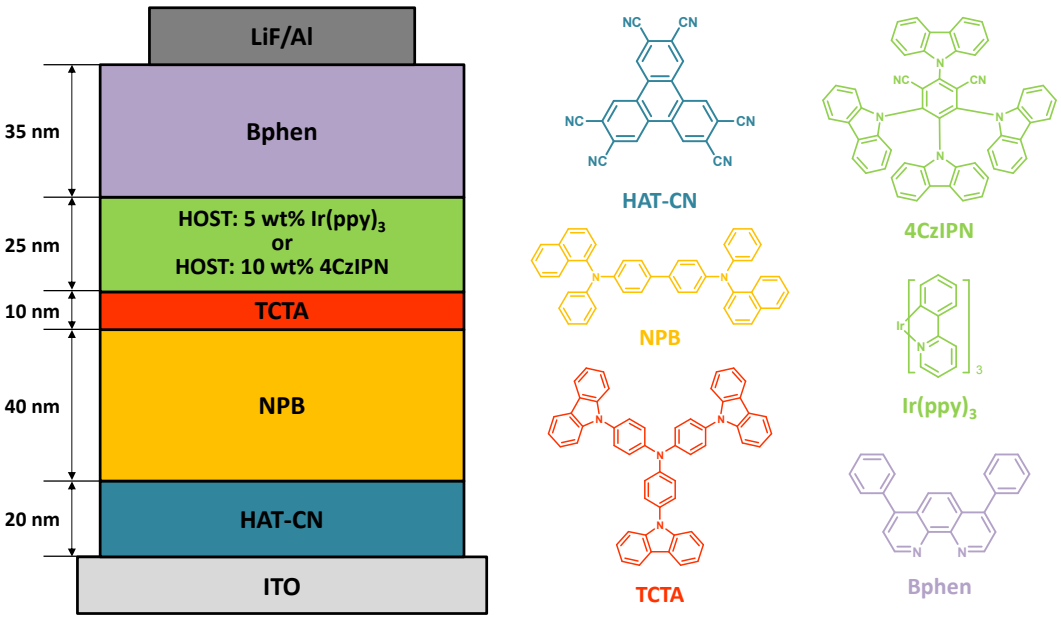

Fig. 7 Device structures of TADF and phosphorescent devices and chemical structures of employed materials.

.

View Article Online
DOI: 10.1039/C7TC00733G

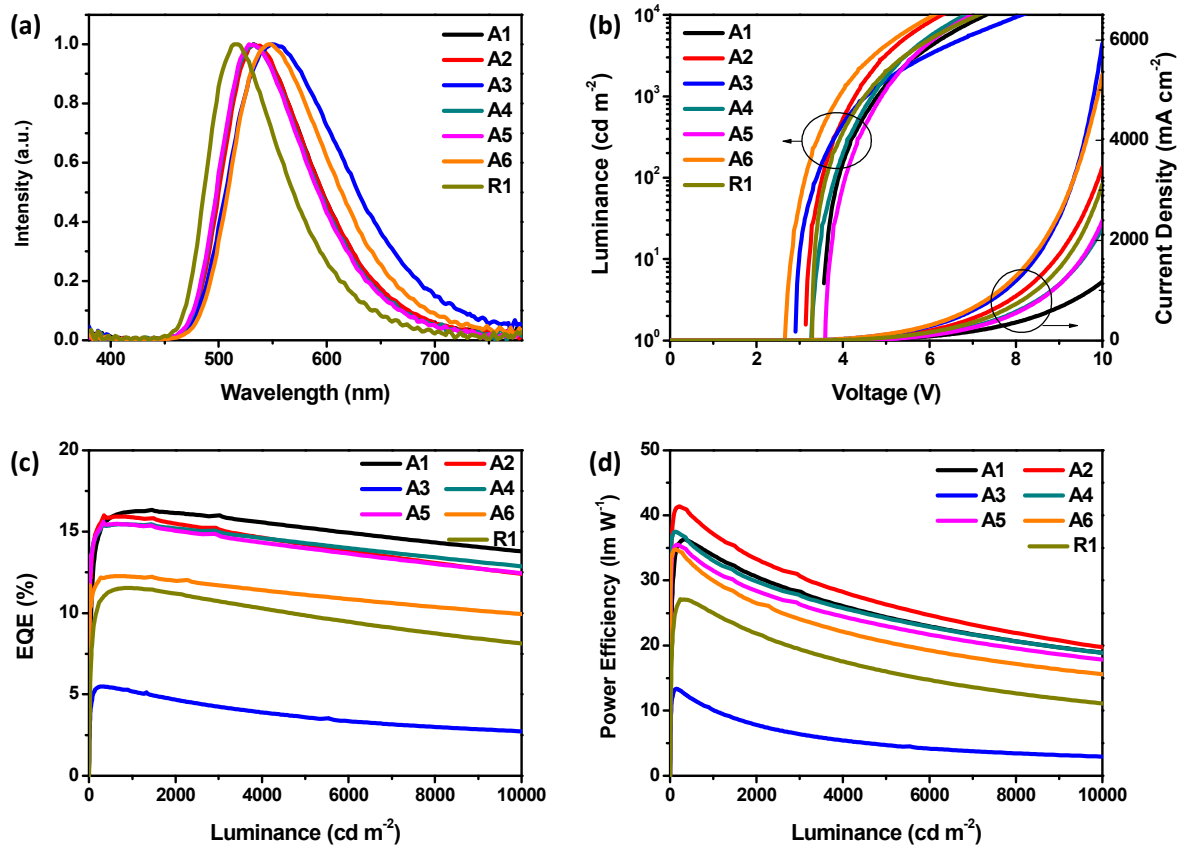

Fig. 8 (a) EL spectra (b) J-V-L characteristics (c) EQEs (d) PEs of TADF OLEDs

View Article Online
DOI: 10.1039/C7TC00733G

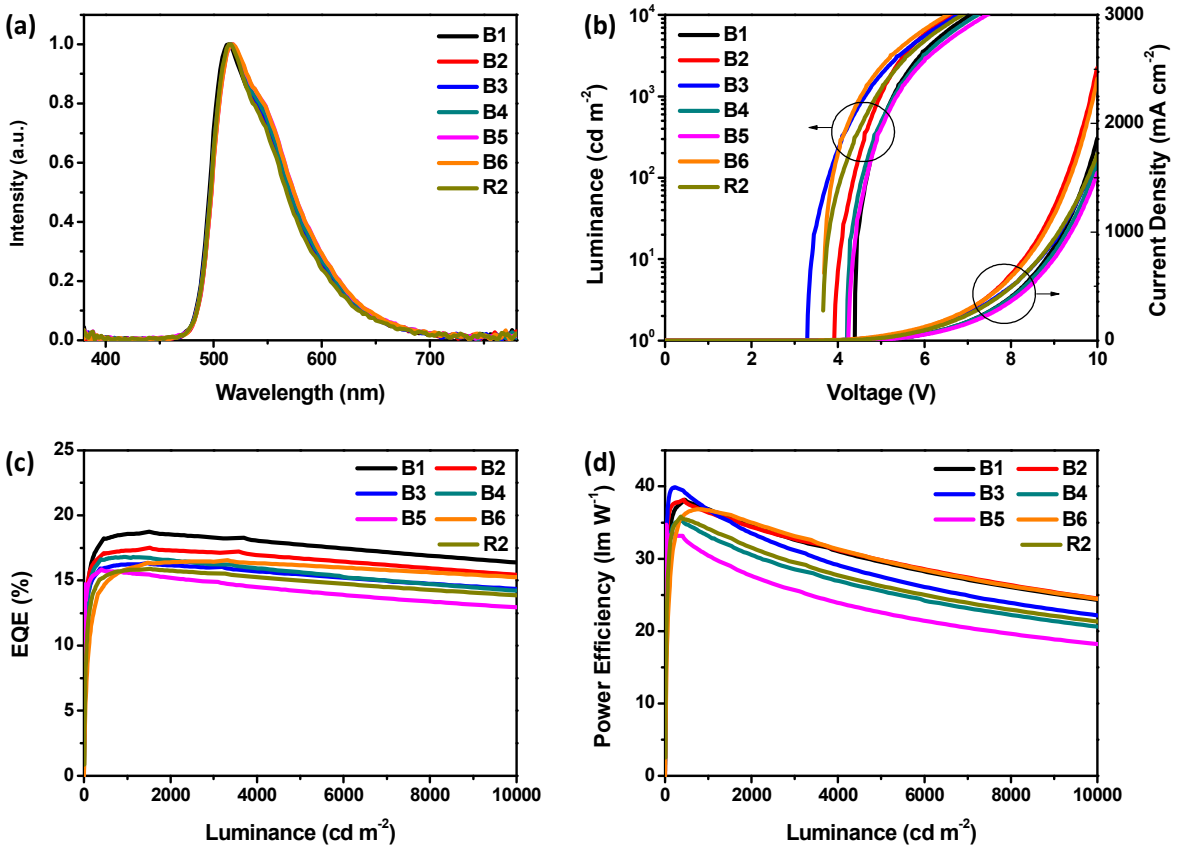

Fig. 9 (a) EL spectra (b) J-V-L characteristics (c) EQEs (d) PEs of PHOLEDs.

View Article Online
DOI: 10.1039/C7TC00733G

Table 1 Physical properties of D1-D6.

Compound	T_d (°C)	T_g (°C)	λ_{Abs} [a] (nm)	λ_{Em} [a] (nm)	HOMO [b] (eV)	LUMO [c] (eV)	T_1 [d] (eV)	μ_h [e] ($cm^2 V^{-1} s^{-1}$)	μ_e [e] ($cm^2 V^{-1} s^{-1}$)
D1	399	102	293, 341	367, 378	5.67	2.10	2.66	5.53×10^{-5}	2.17×10^{-4}
D2	374	111	293	371, 386	5.63	2.13	2.60	2.87×10^{-4}	9.66×10^{-4}
D3	369	107	290	376, 394	5.54	2.10	2.61	4.82×10^{-6}	3.45×10^{-4}
D4	409	124	293, 345	367, 377	5.65	2.10	2.67	5.71×10^{-4}	2.52×10^{-4}
D5	425	114	290, 345	367, 377	5.65	2.08	2.66	1.65×10^{-5}	1.74×10^{-4}
D6	421	120	290, 349	365, 381	5.63	2.18	2.65	8.35×10^{-6}	1.02×10^{-4}

[a] Measured at toluene solution (1×10^{-5} mol L^{-1}), [b] Calculated according to the equation HOMO = 4.8 + onset voltage, [c] Estimated according to the absorption bandgap and the HOMO energy level, [d] Estimated according to the onset of the phosphorescent spectra in toluene solution (1×10^{-5} mol L^{-1}), [e] At 6×10^{7} V m^{-1}.

Table 2 The performances of TADF and phosphorescent devices.

Device	Host	Dopant	V_{on} [a] [V]	EQE [b] (%)	CE [b] (cd/A)	PE [b] (lm/W)
A1	D1	4CzIPN	3.5	16.3/15.3/13.8	51.8/48.6/43.9	36.4/24.4/18.9
A2	D2	4CzIPN	3.1	15.9/14.2/12.4	50.7/45.3/39.6	41.4/26.4/19.8
A3	D3	4CzIPN	2.9	5.5/3.6/2.7	15.4/10.1/7.6	13.3/4.7/3.0
A4	D4	4CzIPN	3.3	15.4/14.3/12.9	49.2/45.6/41.0	37.5/24.3/18.9
A5	D5	4CzIPN	3.6	15.5/14.0/12.4	49.3/44.6/39.6	35.4/23.0/17.8
A6	D6	4CzIPN	2.7	12.3/11.1/9.9	37.4/33.9/30.3	34.8/20.6/15.6
R1	CBP	4CzIPN	3.4	11.5/9.9/8.1	35.8/30.6/25.3	27.1/16.0/11.2
B1	D1	$Ir(ppy)_3$	4.4	18.6/17.6/16.2	62.0/59.2/54.6	37.8/29.6/24.3
B2	D2	$Ir(ppy)_3$	3.9	17.3/16.5/15.3	57.9/55.7/51.6	37.8/29.9/24.6
B3	D3	$Ir(ppy)_3$	3.3	16.2/15.3/14.2	54.2/51.6/47.9	39.9/27.6/22.3
B4	D4	$Ir(ppy)_3$	4.2	16.8/15.5/14.1	56.0/52.1/47.5	35.1/25.6/20.6
B5	D5	$Ir(ppy)_3$	4.3	15.7/14.0/12.8	52.4/47.3/43.2	33.4/22.7/18.1
B6	D6	$Ir(ppy)_3$	3.7	16.4/16.0/15.1	54.8/53.9/50.9	36.8/29.7/24.5
R2	CBP	$Ir(ppy)_3$	3.6	15.8/15.0/13.9	53.3/50.6/46.8	35.5/26.3/21.3

[a] Measured at 1 cd m^{-2}, [b] In the order of Max, 5000 and 10000 cd m^{-2}.

View Article Online
DOI: 10.1039/C7TC00733G

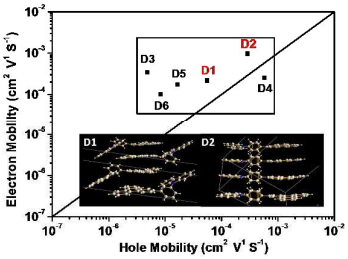

π-π stacking can improve the electron mobilities of bipolar hosts for TADF and phosphorescent devices with low efficiency roll-off